Radiation Physics and Chemistry 239 (2026) 113239

Contents lists available at ScienceDirect

Radiation Physics and Chemistry

journal homepage: www.elsevier.com/locate/radphyschem

Time response of an undoped $LaCl_3$ crystal

M. Caballero [a,*], V. Sánchez-Tembleque [a], L.M. Fraile [a], C. Fonseca-Vargas [b], S. Gaitán [a], H.J. Kim [c], V. Martínez-Nouvilas [a], M. Martínez-Roig [b], E. Nácher [b], J.M. Udías [a], P.Q. Vuong [c]

[a] Grupo de Física Nuclear, EMFTEL & IPARCOS, Facultad de CC. Físicas, Universidad Complutense de Madrid, E-28040 Madrid, Spain
[b] Instituto de Física Corpuscular, CSIC-Universidad de Valencia, E-46980 Valencia, Spain
[c] Department of Physics, Kyungpook National University, Daegu, 41566, South Korea

ARTICLE INFO

Keywords:
Inorganic scintillators
$LaCl_3$
$LaBr_3$(Ce)
Photonis XP2020/URQ photomultiplier tube
Digital signal processing
Time resolution
Time walk
Fast timing

ABSTRACT

We have characterized a detector equipped with an undoped $LaCl_3$ truncated cone crystal with dimensions of 22.5 mm in the largest diameter, 16 mm in the smallest diameter, and 16 mm in height, coupled to a fast Photonis XP2020/URQ photomultiplier tube (PMT). Its time response at 511 keV (^{22}Na) and ^{60}Co photon energies has been measured against a reference detector using a fast digitizer module by digital signal processing methods based on a genetic algorithm. The time resolution was optimized by the choice of the photomultiplier bias voltage and the fine-tuning of the digital parameters of the time pickup algorithm. The de-convoluted full width at half maximum (FWHM) time resolution is found to be 250 ± 10 ps at ^{60}Co energies, and 444 ± 8 ps using positron annihilation γ-rays from ^{22}Na, providing good prospects for the use of the crystal in applications requiring a fast time response.

1. Introduction

High-density fast scintillators have a strong potential for applications requiring high detection efficiency and fast response to γ radiation. Lanthanum halide scintillators (Iltis et al., 2006) fulfill these requirements, since they offer excellent light yield and linear response, leading to very good energy resolution, and also fast scintillation decay components, which make them very well suited for high-counting-rate applications and fast-timing measurements. For these reasons, they have strong potential in applications such as high-energy physics research, medical diagnostics, geological exploration, and diffraction (Knoll, 2010). One of the reasons behind the fast response of lanthanum halide scintillators is the Ce^{3+} doping, which above a certain concentration, contributes to faster pulses with decay times of the order of tens of nanoseconds (Dorenbos, 2000).

One of the fastest inorganic scintillator crystals commercially available nowadays is $LaCl_3$(Ce) (van Loef et al., 2000; Shah et al., 2003). It shows high light yield and proportionality, with a quite fast response, leading to good energy resolution, excellent linearity and fast timing capabilities not far from those of $LaBr_3$(Ce) crystals (Fraile et al., 2020; Vedia et al., 2015b). Pure $LaCl_3$ crystals, without the addition of Ce^{3+} activator, have also been produced (Shah et al., 2003; Pei et al., 2005) with the aim of exploring potential applications in medical imaging and nuclear and particle physics. Crystals of relatively large sizes can be grown by using a modified Bridgman method, achieving good optical transmittance from 300 to 650 nm, and luminescence with a maximum at 405 nm (Pei et al., 2005). The interest of pure $LaCl_3$ crystals mainly resides in the Pulse Shape Discrimination (PSD) capabilities, which makes it possible to distinguish between different types of incident radiation (Harn et al., 2021). This ability is of relevance in different research fields such as national security, safety systems and space exploration (Kouzes et al., 2015; Runkle et al., 2010; Sonu et al., 2023; Feldman et al., 1998).

The number of crystals with PSD capabilities has increased in recent years. Some of them, as the CLYC, the CLLBC, or the TLYC, employ reactions with ^{35}Cl and ^{6}Li to detect γ radiation and neutrons at the same time (D'Olympia et al., 2013). All of them exhibit good light yield, acceptable energy resolution, and a decay with multiple components, with the longest decay time exceeding 1 μs (D'Olympia et al., 2013; Glodo et al., 2013; Arnqvist et al., 2025; Guss et al., 2014; Hawrami et al., 2016; Kim et al., 2016; Hawrami et al., 2017; Vuong et al., 2021, 2022). Moreover, the temporal resolution has been measured for some of them. For CLYC, a value of 495 ps at 511 keV has been reported for ^{22}Na (D'Olympia et al., 2013), while a value of 1170 ps has been measured for CLLBC at ^{60}Co energies (Arnqvist et al., 2025). Other results for different features are reported in Table 1 along with the values previously measured for the $LaCl_3$ crystal (D'Olympia et al.,

* Corresponding author.
E-mail addresses: mirica01@ucm.es (M. Caballero), victosan@ucm.es (V. Sánchez-Tembleque), lmfraile@ucm.es (L.M. Fraile).
URL: http://nuclear.fis.ucm.es (L.M. Fraile).

https://doi.org/10.1016/j.radphyschem.2025.113239
Received 16 June 2025; Received in revised form 5 August 2025; Accepted 10 August 2025
Available online 22 August 2025

Table 1
Summary of properties of crystals with PSD properties.

Crystal	Light yield (ph/MeV)	Energy resolution (%) at 662 keV	Decay time (μs)
CLYC	20 000	<4.0	0.3, 0.7, 5.2
CLLBC	40 000	4.1	0.09, 0.3, 1.4
TLYC	>26 000	>4.0	0.06, 0.4, 1.1
$LaCl_3$	34 000	4.9	3.3

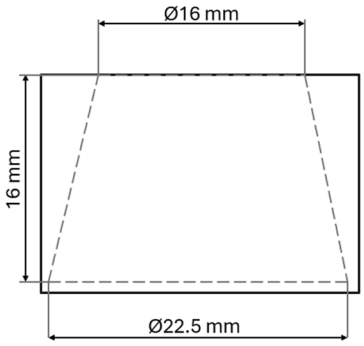

Fig. 1. Dimensions of the $LaCl_3$ crystal.

2013; Glodo et al., 2013; Arnqvist et al., 2025; Guss et al., 2014; Hawrami et al., 2016; Kim et al., 2016; Hawrami et al., 2017; Vuong et al., 2021, 2022).

While PSD is an asset, the lack of Ce activation centers depletes the light yield and extends the decay time compared to $LaCl_3$(Ce) crystals. For Ce concentrations below 1%, the main light emission peak is shifted above 400 nm and the dominant decay time constant is larger than 200 ns (van Loef et al., 2000; Shah et al., 2003). Although undoped $LaCl_3$ may not match the energy resolution and time response observed in $LaCl_3$(Ce), it may still remain a competitive choice for applications requiring fast time response or high count rate capabilities, which may add to the PSD potential.

In this paper, we evaluate the performance of a $LaCl_3$ crystal with the shape of a truncated cone, assessing its linearity, energy resolution and efficiency, and with a special focus on its time response. To this end we have performed coincidence experiments to measure the de-convoluted FWHM time resolution against a well-characterized reference $LaBr_3$(Ce) detector.

2. Materials and methods

2.1. The $LaCl_3$ detector assemblies

The $LaCl_3$ crystal used was produced in the Kyungpook National University, Daegu, Korea, with the shape of a truncated cone. Its largest diameter size is 22.5 mm, its smallest diameter is 16 mm and its height is 16 mm, as illustrated in Fig. 1. This geometry has shown to provide good time performance for BaF_2 and $LaBr_3$(Ce) crystals (Moszynski et al., 2003; Vedia et al., 2015a).

As discussed above, the photoemission of $LaCl_3$ peaks around 405 nm, and it is transparent in the 300 to 600 nm wavelength range with the transmission of the order 80% (Pei et al., 2005). Due to the hygroscopic nature and water solubility of lanthanum chloride, the $LaCl_3$ crystal is enclosed in an airtight aluminum container with a reduced entrance thickness and a quartz window on the coupling side.

Two different photomultiplier tubes (PMTs) have been used. For the assessment of the PSD capabilities, a $LaCl_3$-PMT assembly with a Hamamatsu R1924A-100 PMT was employed. The R1924A-100 is a one-inch head-on 10-stage PMT with an effective diameter of 22 mm and a super bi-alkali photocathode. It operates in the 300 to 650 nm spectral range. Its main features are summarized in Table 2.

Table 2
Summary of main properties of the PMTs used in this work in combination with the $LaCl_3$ crystal.

Parameter	R1924A-100	XP2020-URQ
τ_{rise} (ns)	1.5	1.6
Electron transit time (ns)	17	30
Transit time spread σ (ps)	900	250
Cathode sensitivity (μA/lmF)	90	70
Blue sensitivity (μA/lmF)	10.5	10
Blue sensitivity (μA/lmF)	10.5	10
Dark current (nA)	3	20
Gain	2×10^6	3×10^7

For the rest of the assessment of the detector, and for the fast-timing measurements in particular, we used an XP2020-URQ PMT by Photonis, a 2-inch 12-stage head-on device. It is known for its good timing performance, which is specifically due to its anode pulse rise time of 1.6 ns, and has a FWHM Transit Time Spread of 250 ps (Photonis, 2025), see Table 2. It is fitted with a quartz window, and its minimum effective diameter is 44 mm. It operates also in the ultraviolet with an extended 160 to 650 nm spectral range. In addition to its fast response, it features high gain, of the order of 3×10^7.

2.2. Experimental set-up

Fast-timing measurements were performed with a time-delayed coincidence set-up similar to the one described in Vedia et al. (2015b,a), Sánchez-Tembleque et al. (2019). It consisted of a reference $LaBr_3$(Ce) detector composed of a truncated cone crystal of 1.5“ in height, 1.5” in its largest diameter, and 1” in its smallest diameter (Sánchez-Tembleque et al., 2019), which was coupled to a Hamamatsu R9779 PMT operated at −1275 V and had been previously optimized for the best timing performance, and the $LaCl_3$ under test coupled to the Photonis XP2020-URQ PMT presented above. Both detectors were positioned facing each other at a separation distance of 21 mm between their entrance faces, with the radiation source placed midway in between. Measurements were performed using ^{60}Co and ^{22}Na γ-ray sources, employing the 1173–1332 keV pair, whose excited state lifetime is 0.9 ± 0.3 ps (Browne and Tuli, 2013), and the annihilation 511-keV radiation, respectively. For the^{22}Na source, the excited state lifetime is 3.60 ± 0.05 ps (Basunia, 2015), while the positronium lifetime in the encapsulating material is expected to range between 2.0 and 2.1 ns (Ernst and Randolph, 1997). The time resolution of the reference $LaBr_3$(Ce) detector was measured using three detectors grouped in pairs, following the procedures described in Vedia et al. (2015b). The de-convoluted FWHM time resolution values were found to be 116 ± 4 ps for the ^{60}Co full-energy peaks and 157 ± 3 ps for the 511-keV photons from the ^{22}Na source. These will be used throughout the paper. The reference detector has a significantly better time resolution than the values reported below for $LaCl_3$ so it should not affect the results.

2.3. Timing measurements

For the timing measurements, we chose a data acquisition based on the PSI DRS digitizer (Institute, 2025; Ritt et al., 2010) due to its 5.12 GSa/s sampling rate and 750 MHz bandwidth, which has already been proven to be well suited for fast-timing (Fraile et al., 2020; Sánchez-Tembleque et al., 2019). An internal logical AND trigger implemented in the DRS chip was used to record coincidence events. Pulse traces were recorded and digital signal processing methods were used offline to determine the pick-up time in order to define the signal timestamps.

The signal processing method described in Sánchez-Tembleque et al. (2019) includes a filtering stage and the implementation of a pick-up algorithm, which are both optimized using the procedure ased on a genetic algorithm. The filter makes use of a digital recursive filter shown in Eq. (1), where V is the voltage for a given sample before applying the digital filter, and $\tilde{V}$ is the resulting voltage after applying the filter. The optimized digital filter has been shown to improve the time pickup, and thus the time resolution results (Sánchez-Tembleque et al., 2019).

$$\tilde{V}[n] = A \cdot \tilde{V}[n-1] + B \cdot V[n] + C \cdot V[n-1] \quad (1)$$

Several algorithms may be used to determine pulse time pick up (Sánchez-Tembleque et al., 2019). Owing to the irregularity of the $LaCl_3$ signals, which show different shapes for similar amplitudes where the absolute maximum is not always the local maximum of the initial signal rise (see Section 3.2), a constant fraction discriminator algorithm seems appropriate. Such a constant fraction discriminator algorithm, implemented fully in digital (DCFD) (Jäger and Butz, 2012) provides pickup times independent from the pulse amplitude. The DCFD mimics the procedure of an analog CFD by combining an inverted fraction of the input signal with its delayed copy and finding the zero crossing of the resulting bipolar pulse. Therefore it depends on the fraction and the time delay, which are used as parameters for the optimization. Both the DCFD and the filter parameters were optimized using the genetic algorithm.

Alternative methods, such as a fully digital constant fraction implemented as a Relative Digital Leading Edge Discriminator (RDLED) (Sánchez-Tembleque et al., 2019), may suffer from difficulties in finding the absolute maximum of the pulse, while an absolute Digital Leading Edge Discriminator (DLED) (Sánchez-Tembleque et al., 2019) will be subject to variations depending on the signal amplitude.

Once the pick-up time was obtained for both the reference and the $LaCl_3$(Ce) detectors, time difference spectra were constructed. Coincidence gates were applied based on the energy spectra. For the ^{60}Co source, gates were set at 1332- and 1173-keV energies by selecting the Full Width at Tenth Maximum (FWTM). The time difference spectra were limited to events within the energy coincidence windows. In this case, two separate time spectra were generated, one with the 1173-keV condition in the $LaCl_3$ and the 1332-keV one in $LaBr_3$(Ce), and the other with exchanged energies between detectors. Afterward, both were combined, once corrected for energy–time walk, and the coincidence time resolution (CTR) was calculated as the FWHM of the resulting time spectrum. Similarly, gates for ^{22}Na were placed around the 511-keV full-energy peak in each detector by selecting the FWTM. The time resolution is given as the FWHM of the obtained time spectrum. De-convoluted FWHM values are also provided for the $LaCl_3$ detector.

2.4. Energy and efficiency measurements

Additionally, a desktop CAEN DT5720b 12-bit 250 MS/s ADC digitizer (CAEN, 2025) was employed to measure the energy resolution and linearity of the $LaCl_3$ detector, profiting from the possibility of using longer integration windows. Energy spectra were acquired for ^{22}Na, ^{60}Co, ^{137} Cs and ^{152}Eu standard sources. Selected full-energy γ peaks were identified, establishing the energy-channel relationship at different voltage settings for the $LaCl_3$ detector in order to determine the linearity. Furthermore, energy resolution and efficiency were measured from these spectra. The distance between the source and detector was fixed at 10 mm for energy resolution measurements, while for efficiency assessments, the source was positioned at distances of 50 mm, 30 mm, 20 mm, 15 mm, and 10 mm from the detector entrance window.

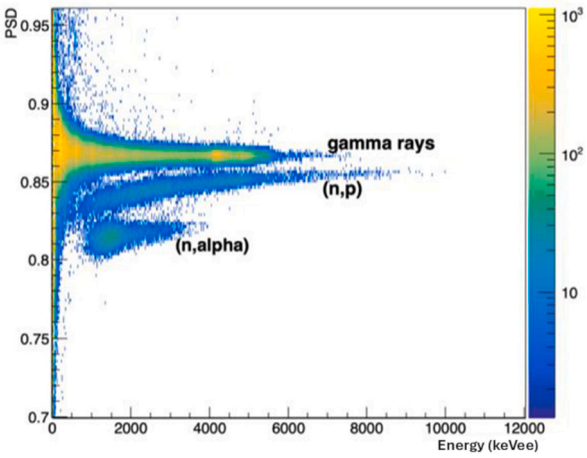

Fig. 2. Illustration of PSD capabilities of the $LaCl_3$ crystal.

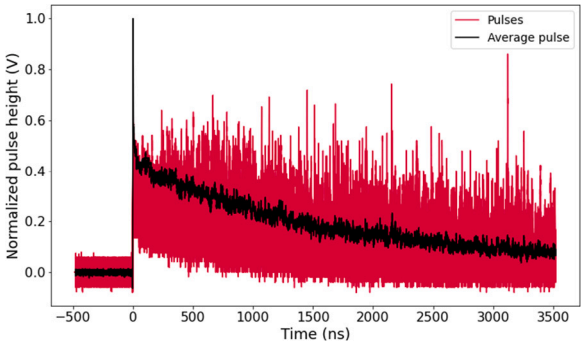

Fig. 3. Normalized positive cathode pulses measured for the $LaCl_3$ crystal coupled to the Photonis XP2020-URQ PMT. The collected pulse data is represented by a red line, while the mean signal is depicted in black.

3. Results and discussion

3.1. Pulse-shape discrimination

An illustration of the PSD capability of the $LaCl_3$ crystal coupled to the R1924A-100 Hamamatsu PMT is presented in Fig. 2. The measurement was carried out at CMAM (Redondo-Cubero et al., 2021) using an ^{27}Al(α,n) reaction, which leads to the production of γ rays along with the neutrons. Three sets of different particles can be distinguished in the figure, γ-rays, protons and alpha particles, both charged particles produced by neutrons reaching the detector. Successful discrimination is achieved when a very long integration window of the order of 10 μs is employed.

3.2. Detector output signals

We discuss below results using the $LaCl_3$-XP2020 detector, with the XP2020-URQ Photonis PMT operated at the voltage of −2600 V, for γ radiation. The positive (cathode) output pulses from the detector were examined with the help of a fast RTO6 oscilloscope by Rohde& Schwarz (Schwarz, 2025). Normalized pulses are presented in Fig. 3, where the very fast rise time of the order of 1 ns is apparent, together with a long decay of few μs. In principle, the fast rise time holds the potential for a fast response of the crystal, although it will be a challenge to simultaneously achieve PSD. A small undershoot is observed in the signal. It is also noticeable that signals are not always regular and they exhibit varying rise times for similar amplitudes, as discussed above.

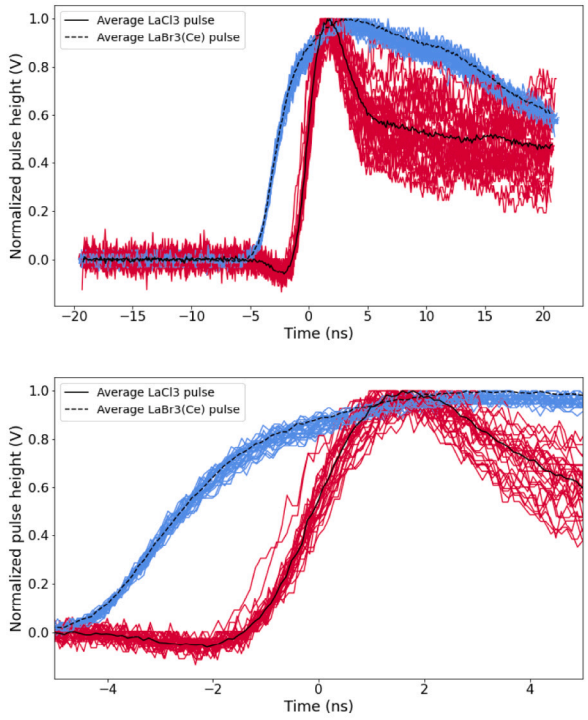

Fig. 4. Comparison between $LaCl_3$ pulses and $LaBr_3$(Ce) pulses. Experimental data in blue represents $LaBr_3$(Ce) pulses while red color corresponds to $LaCl_3$ pulses, both for the 1332-keV full-energy peak. Averaged signals are shown by black lines. A zoom on the pulse rise is provided below.

To explore this further, a close-up is presented in Fig. 4, where the sharp rise time is compared to the reference $LaBr_3$(Ce) detector. The decay of the $LaCl_3$ pulses is also complex, with a weak but very fast decay with τ_{fast} ~5.5 ns, and at least two slow components: one with τ_{medium} = 717 ± 4 ns, and a second much longer component with τ_{slow} = 3.211 ± 0.014 μs, obtained from a multiple exponential fit of the average output pulses.

3.3. Linearity, energy resolution and efficiency

Plots from Fig. 5 show the energy spectra obtained for ^{152}Eu and ^{137}Cs sources at a distance of 10 mm to the detector entrance window and with the XP2020-URQ PMT operated at −2300 V. The CAEN digitizer was used for this purpose, as discussed in Section 2.4.

The linearity has been assessed as a function of the applied high voltage from −2200 V to −2600 V. Results are shown in Fig. 6. For these measurements sources of ^{22}Na, ^{60}Co, ^{137}Cs and ^{152}Eu were used. A linear energy calibration was performed using the ^{152}Eu full-energy peaks at 121.8, 244.7 and 344.3 keV, and then applied to calculate the extrapolated channel for the 1332-keV FEP in ^{60}Co. The non-linearity is estimated as the relative deviation of the extrapolated channel with respect to the actual one measured at 1332 keV.

The non-linearity remains below 2.5% for every tested voltage in the range 122 to 1332 keV and does not increase with the applied voltage. Thus the $LaCl_3$(Ce)-XP2020URQ detector shows a relatively linear behavior at the operation voltages.

The relative energy resolution R, given as the FHWM to centroid ratio in keV in %, is shown as a function of energy in Fig. 7 for selected FEP from standard sources. The ^{137}Cs FWHM energy resolution, once corrected for non-linearity, is 7.4%. As expected, the relative E resolution improves with energy. A fit following Eq. (2)

$$R = a + \frac{b}{E}, \tag{2}$$

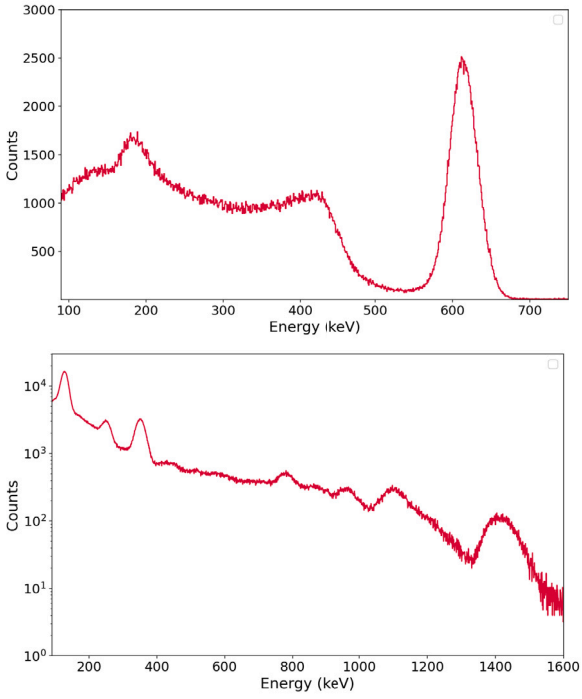

Fig. 5. Above: energy spectrum for a ^{137}Cs source observed in the $LaCl_3$-XP2020URQ detector operated at HV = −2300V. Below: energy spectrum for ^{152}Eu, shown in logarithmic scale.

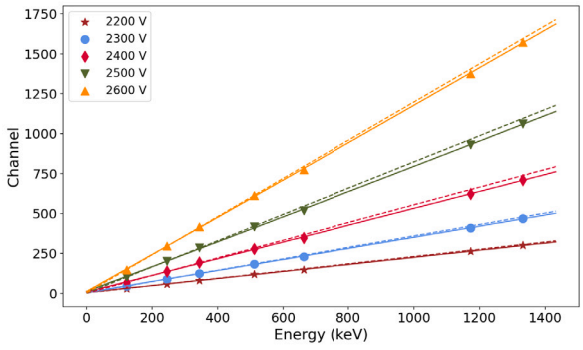

Fig. 6. Energy linearity plots for the $LaCl_3$Photonis detector. For each HV value the dashed line illustrates linear interpolation using energies solely within the range from 122 to 344 keV, while continuous lines depict a quadratic fit for all points.

where E denotes the energy in keV, R represents the resolution, and a and b are free parameters, was performed, resulting in a=5.13(6)% and b= 1569(15)% keV.

The FEP efficiency has been also measured as a function of the distance between the source and the $LaCl_3$-Photonis detector operated at −2300 V. Spectra were measured for an absolutely calibrated ^{152}Eu source at distances of 10 mm, 15 mm, 20 mm, 30 mm, and 50 mm using the CAEN digitizer. Results are presented in Fig. 8. Data were collected for 1800 s at distances of 10 mm and 15 mm, and for the remaining distances for 50400 s. The contributions of the room background were subtracted. The absolute efficiency at 20 mm from the entrance window is 2.5(3)% at 122 keV and 0.074(9)% at 1408 keV.

3.4. Time response

The time response of the $LaCl_3$-XP2020URQ detector was investigated using the DRS digitizer (see Section 2.3), operated at a sampling rate of 5.12 GSa/s.

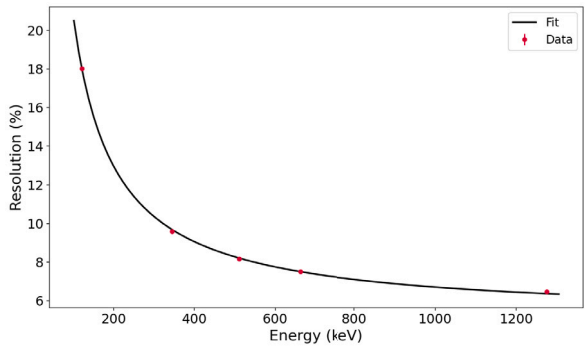

Fig. 7. Relative energy resolution for ^{22}Na, ^{60}Co, ^{137}Cs and ^{152}Eu sources at 10 mm observed in the $LaCl_3$ Photonis detector operated at HV = −2300V at 10 mm. Error bars are smaller that the data points. A fit to expression (2) is also shown.

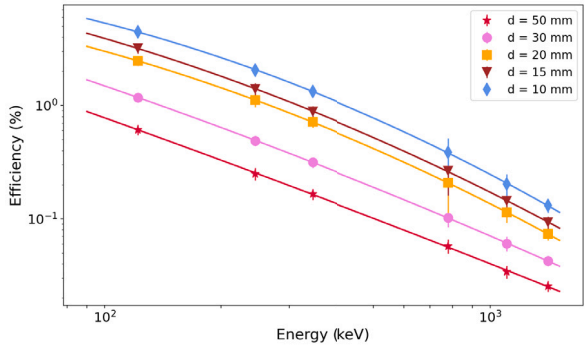

Fig. 8. Efficiency plots for the $LaCl_3$-Photonis detector, operated at − 2300 V. The experimental values are depicted by points, while the lines represent a fit to the data.

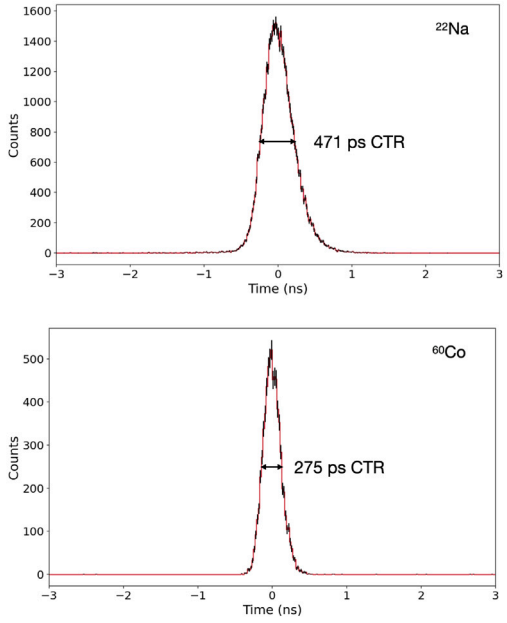

Fig. 9. Time spectrum for $LaCl_3$ Photonis detector at −2600 V against the reference detector at −1275 V measured with ^{22}Na source (top panel). The spectra are represented in red with black error bars.

Firstly, energy windows defined at the full width at one-tenth of maximum were selected for relevant full-energy peaks, the 1173- and 1332-keV ones for^{60}Co, and the 511-keV FEP for the^{22}Na source. Then,

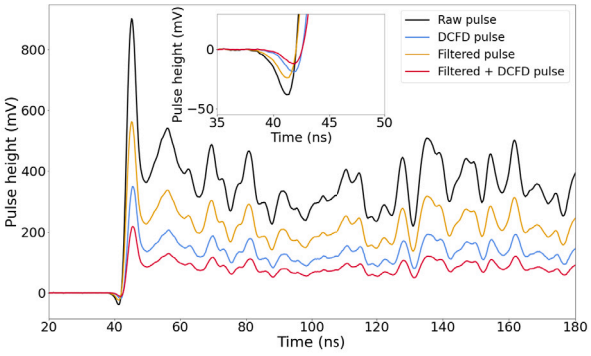

Fig. 10. The successive stages of signal processing applied to a single pulse are illustrated. The black line corresponds to the unprocessed pulse. The yellow pulse shows the effect of applying a filter. The red trace depicts the product of sequentially applying both the filter and the DCFD to the initial signal. For completeness, the result of applying the DCFD algorithm to the raw signal is represented in blue. The inset provides a zoom into the zero-crossing region.

an optimization of the applied voltage was carried out. Our analysis revealed that the time resolution improved with increasing voltage, with the most favorable results observed at −2600 V. The results below are thus provided at this HV value.

The procedures described in Section 2.3 were applied to find the optimum parameters both for the generalized filter and the DCFD. Fig. 10 illustrates a $LaCl_3$(Ce) pulse at different processing stages. As shown, the DCFD has also been applied to the raw pulse in order to investigate the effect of the digital filter. It is observed that the effect of the generalized filter in the time resolution is marginal, with no sizeable contribution at^{60}Co energies and an improvement of approximately 5% at 511 keV. The best results using the Digital CFD are achieved with a fraction of 62%, and a time delay of 349 ps. This indicates that the DCFD makes it possible to define time stamps from the first scintillation photon. As shown in Fig. 10, the large fraction and very short delay obtained, imply that the zero-crossing of the DCFD processed signal reverts to the pulse undershoot. As a cross-check, the RDLED and DLED methods (thresholds relative to maximum and absolute) were also tried using the genetic algorithm optimization, leading to similar or slightly worse results than the DCFD.

FWHM time difference spectra using the DCFD method for ^{60}Co and ^{22}Na are presented in Fig. 9. The time distributions have a Gaussian shape, although the one for the 511-keV full-energy peak is slightly asymmetric. The FWHM resolution of 471 ps from the ^{22}Na spectrum includes the individual contributions from the reference detector of 157 ± 3 ps and the $LaCl_3$ unit of 444 ± 8 ps, while the ^{60}Co CTR of 275 ps is given by the individual contributions from the reference detector of 116 ± 4 ps and the $LaCl_3$ unit of 250 ± 10 ps. These are the final, optimized values, achieved for the $LaCl_3$(Ce) detector. Uncertainties were evaluated by a bootstrapping procedure: each acquisition was randomly split into two subsets, and the CRT was recalculated for both. This procedure was repeated 100 times, resulting in 200 FWHM measurements. The standard deviation for the distribution of the 200 FWHM values is the reported uncertainty.

It is worth mentioning that we have investigated the time resolution with an increased sampling rate using a R&S®RTO6 oscilloscope (Schwarz, 2025) at 10 GSa/s, with no sizeable time resolution improvement.

Additionally, we have studied the Compton time walk for ^{60}Co. Centroid values of time spectra were acquired by setting different energy windows on the $LaCl_3$ detector while maintaining a constant energy window on the $LaBr_3$(Ce) detector defined at FWTM of the 1332-keV FEP. Results are presented in Fig. 11 for the Compton and FEP from the 1173-keV peak. It is worth noting that the response is very flat, the time walk in the range 50 to 1250 keV being only 150 ps, including the backscattered component.

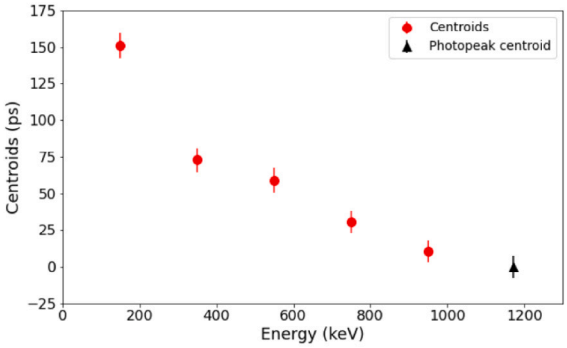

Fig. 11. Compton time walk for the $LaCl_3$ detector using a ^{60}Co source. Time-difference centroid positions in ps are represented against energy. Dots are positioned at the midpoint of the selected 200-keV-wide energy gate. Red circles represent the centroid of the Compton energies, while the black triangle shows the centroid from the 1173-keV FEP.

4. Summary and conclusions

We have characterized the performance of a detector system consisting of an undoped $LaCl_3$ crystal with the shape of a truncated cone coupled to the XP2020Q/UR Photonis photomultiplier, with particular emphasis on measuring its time response.

The energy response of the $LaCl_3$-XP2020-URQ detector is found to be very linear. We also report a relatively good energy resolution of 7.4% for the 662-keV full-energy peak from ^{137}Cs and 6.1% at 1332-keV energies from a ^{60}Co source.

Once the applied high voltage is optimized, a good time resolution is obtained using a DCFD, a Constant Fraction Discriminator algorithm implemented digitally. A FWHM of 250 ± 10 ps was obtained at ^{60}Co energies, while the value obtained for ^{22}Na 511-keV photons is 444 ± 8 ps.

Together with its PSD capabilities, our results show that undoped $LaCl_3$ is a promising inorganic crystal for applications requiring spectroscopic capabilities and good time resolution. However, output pulses are very long, and integration over very long times is required for both peak-height analysis and the implementation of pulse-discrimination, which may hamper in particular high-rate experiments.

CRediT authorship contribution statement

M. Caballero: Writing – review & editing, Writing – original draft, Software, Methodology, Investigation, Formal analysis, Data curation. **V. Sánchez-Tembleque:** Writing – review & editing, Validation, Supervision, Software, Methodology, Investigation. **L.M. Fraile:** Writing – review & editing, Validation, Supervision, Resources, Project administration, Methodology, Funding acquisition, Conceptualization. **C. Fonseca-Vargas:** Investigation, Formal analysis. **S. Gaitán:** Investigation. **H.J. Kim:** Resources. **V. Martínez-Nouvilas:** Software, Investigation. **M. Martínez-Roig:** Investigation. **E. Nácher:** Resources, Project administration, Funding acquisition. **J.M. Udías:** Software, Project administration, Funding acquisition. **P.Q. Vuong:** Resources.

Declaration of Generative AI and AI-assisted technologies in the writing process

During the preparation of this work the authors used ChatGPT in order to improve the readability. After using this tool/service, the authors reviewed and edited the content as needed and take full responsibility for the content of the publication.

Declaration of competing interest

The authors declare that they have no known competing financial interests or personal relationships that could have appeared to influence the work reported in this paper.

Acknowledgments

We acknowledge support from the Spanish MCIN/AEI/10.13039/501100011033 via PID2021-126998OB-I00, TED2021-130592B-I00 and PDC2022-133382-I00 projects, and by the HISTARS CERN-MRR project funded by the Spanish MCIN and the European Union NextGenerationEU RRF. We also acknowledge funding by *Tecnologías Avanzadas para la Exploración del Universo y sus Componentes* (PR47/21 TAU-CM TAU-PRTR) project, funded by the Spanish MCIN, Comunidad de Madrid (Spain) and the European Union NextGenerationEU RRF. Finally, E. Nácher and C. Fonseca thank the funding from the Generalitat Valenciana, Spain through grant CIPROM/2021/064.

Data availability

Data will be made available on request.

References

Arnqvist, E., Oberstedt, S., Al-Adili, A., Fontana, C.L., Borella, A., Rossa, R., Geerts, W., Macías, M., Vidali, M., Oberstedt, A., Lantz, M., 2025. Characterization of CLLBC scintillation detector response to γ-rays and neutrons. Nucl. Instrum. Methods Phys. Res. Sect. A: Accel. Spectrometers Detect. Assoc. Equip. 1076, 170470. http://dx.doi.org/10.1016/j.nima.2025.170470.

Basunia, M.S., 2015. Adopted Levels and Gammas for ^{22}Ne. National Nuclear Data Center, Brookhaven National Laboratory, Evaluated via ENSDF, https://www.nndc.bnl.gov/ensnds/22/Ne/adopted.pdf.

Browne, E., Tuli, J.K., 2013. Beta Decay Data Sheet for ^{60}Ni. National Nuclear Data Center, Brookhaven National Laboratory, Evaluated via ENSDF, https://www.nndc.bnl.gov/ensnds/60/Ni/beta_decay_1925.28_d.pdf.

CAEN, 2025. DT5720 desktop digitizer. https://www.caen.it/products/dt5720/.

D'Olympia, N., Chowdhury, P., Lister, C., Glodo, J., Hawrami, R., Shah, K., Shirwadkar, U., 2013. Pulse-shape analysis of CLYC for thermal neutrons, fast neutrons, and γ-rays. Nucl. Instrum. Methods Phys. Res. Sect. A: Accel. Spectrometers Detect. Assoc. Equip. 714, 121–127. http://dx.doi.org/10.1016/j.nima.2013.02.043.

Dorenbos, P., 2000. 5D-level energies of Ce^{3+} and the crystalline environment, and iodide compounds. Phys. Rev. B 62 (23), 650–659. http://dx.doi.org/10.1103/PhysRevB.62.15640.

Ernst, W.G., Randolph, J.A., 1997. Life-cycle assessment of ethylene-propylene rubber compounds. Polym. Eng. Sci. 37 (8), 1220–1230. http://dx.doi.org/10.1002/pen.10461.

Feldman, W.C., Maurice, S., Binder, A.B., Barraclough, B.L., Elphic, R.C., Lawrence, D.J., 1998. Fluxes of fast and epithermal neutrons from lunar prospector: Evidence for water ice at the lunar poles. Science 281 (5382), 1496–1500. http://dx.doi.org/10.1126/science.281.5382.1496.

Fraile, L.M., Sánchez-Tembleque, V., Benito, J., García-Díez, M., Udías, J.M., Vedia, V., 2020. Advanced scintillators for fast-timing applications. Nucl. Instrum. Methods Phys. Res. Sect. B: Beam Interactions Mater. Atoms 463, 394–397. http://dx.doi.org/10.1016/j.nimb.2019.04.044.

Glodo, J., Hawrami, R., Shah, K.S., 2013. Development of Cs_2LiYCl_6 scintillator. J. Cryst. Growth 379, 73–78. http://dx.doi.org/10.1016/j.jcrysgro.2013.03.023, Compound Semiconductors and Scintillators for Radiation Detection Applications: A Special Tribute to the Research of Michael Schieber.

Guss, P.P., Stampahar, T.G., Mukhopadhyay, S., Barzilov, A., Guckes, A., 2014. Scintillation properties of a Cs_2LiLa (Br_6) 90%(Cl_6) 10%: Ce_3+ (CLLBC) crystal. In: Radiation Detectors: Systems and Applications XV, vol. 9215, SPIE, pp. 27–41. http://dx.doi.org/10.1117/12.2060204.

Harn, R., Osovizky, A., Kadmon, Y., Manor, A., Ghelman, M., 2021. Analog pulse shape discrimination based on time duration and pulse height. EPJ Web Conf. 253, 11008. http://dx.doi.org/10.1051/epjconf/202125311008.

Hawrami, R., Ariesanti, E., Soundara-Pandian, L., Glodo, J., Shah, K.S., 2016. Tl_2LiYCl_6:Ce: A new elpasolite scintillator. IEEE Trans. Nucl. Sci. 63 (6), 2838–2841. http://dx.doi.org/10.1109/TNS.2016.2627523.

Hawrami, R., Ariesanti, E., Wei, H., Finkelstein, J., Glodo, J., Shah, K., 2017. Tl_2LiYCl_6: Large diameter, high performing dual mode scintillator. Cryst. Growth Des. 17 (7), 3960–3964. http://dx.doi.org/10.1021/acs.cgd.7b00583.

Iltis, A., Mayhugh, M.R., Menge, P., Rozsa, C.M., Selles, O., Solovyev, V., 2006. Lanthanum halide scintillators: Properties and applications. Nucl. Instrum. Methods Phys. Res. Sect. A: Accel. Spectrometers Detect. Assoc. Equip. 563 (2), 359–363. http://dx.doi.org/10.1016/j.nima.2006.02.192, TRDs for the Third Millenium.

Institute, P.S., 2025. DRS chip home page. https://www.psi.ch/en/drs.

Jäger, M., Butz, T., 2012. FPGA implementation of digital constant fraction algorithm with fractional delay for optimal time resolution. Nucl. Instrum. Methods Phys. Res. Sect. A: Accel. Spectrometers Detect. Assoc. Equip. 674, 24–27. http://dx.doi.org/10.1016/j.nima.2012.01.022.

Kim, H.J., Rooh, G., Park, H., Kim, S., 2016. Tl_2LiYCl_6 (Ce^3 +): New Tl-based elpasolite scintillation material. IEEE Trans. Nucl. Sci. 63 (2), 439–442. http://dx.doi.org/10.1109/TNS.2016.2530822.

Knoll, G.F., 2010. Radiation Detection and Measurement, fourth ed. Wiley, New York, NY.

Kouzes, R.T., Lintereur, A.T., Siciliano, E.R., 2015. Progress in alternative neutron detection to address the helium-3 shortage. Nucl. Instrum. Methods Phys. Res. Sect. A: Accel. Spectrometers Detect. Assoc. Equip. 784, 172–175. http://dx.doi.org/10.1016/j.nima.2014.10.046, Symposium on Radiation Measurements and Applications 2014 (SORMA XV).

van Loef, E.V.D., Dorenbos, P., van Eijk, C.W.E., Krämer, K., Güdel, H.U., 2000. High-energy-resolution scintillator: Ce^{3+} activated $LaCl_3$. Appl. Phys. Lett. 77 (10), 1467–1468. http://dx.doi.org/10.1063/1.1308053.

Moszynski, M., Kapusta, M., Wolski, D., Balcerzyk, M., Flyckt, S., Lavoute, P., Mannonier, C., Mach, H., 2003. New fast photomultipliers with a screening grid at the anode. In: 2003 IEEE Nuclear Science Symposium. Conference Record (IEEE Cat. No.03CH37515), vol. 2, pp. 1378–1383 Vol.2. http://dx.doi.org/10.1109/NSSMIC.2003.1351950.

Pei, Y., Chen, X., Mao, R., Ren, G., 2005. Growth and luminescence characteristics of undoped $LaCl_3$ crystal by modified bridgman method. J. Cryst. Growth 279 (3), 390–393. http://dx.doi.org/10.1016/j.jcrysgro.2005.02.034.

Photonis, 2025. Photobultiplier Tubes: Product Specification XP2020/URQ. Tech. rep., Photonis imaging sensors.

Redondo-Cubero, A., Borge, M.J.G., Gordillo, N., Gutiérrez, P.C., Olivares, J., Pérez Casero, R., Ynsa, M.D., 2021. Current status and future developments of the ion beam facility at the centre of micro-analysis of materials in madrid. Eur. Phys. J. Plus 136 (2), 175. http://dx.doi.org/10.1140/epjp/s13360-021-01085-9.

Ritt, S., Dinapoli, R., Hartmann, U., 2010. Application of the DRS chip for fast waveform digitizing. Nucl. Instrum. Methods Phys. Res. Sect. A: Accel. Spectrometers Detect. Assoc. Equip. 623 (1), 486–488. http://dx.doi.org/10.1016/j.nima.2010.03.045.

Runkle, R.C., Bernstein, A., Vanier, P.E., 2010. Securing special nuclear material: Recent advances in neutron detection and their role in nonproliferation. J. Appl. Phys. 108 (11), 111101. http://dx.doi.org/10.1063/1.3503495.

Sánchez-Tembleque, V., Vedia, V., Fraile, L.M., Ritt, S., Udías, J.M., 2019. Optimizing time-pickup algorithms in radiation detectors with a genetic algorithm. Nucl. Instrum. Methods Phys. Res. Sect. A: Accel. Spectrometers Detect. Assoc. Equip. 927, 54–62. http://dx.doi.org/10.1016/j.nima.2019.02.017.

Schwarz, R.., 2025. R&s (r) RTO6 oscilloscope series. https://scdn.rohde-schwarz.com/ur/pws/dl_downloads/pdm/cl_brochures_and_datasheets/specifications/5216_1640_22/RTO6_specs_en_5216-1640-22_v1300.pdf.

Shah, K.S., Glodo, J., Klugerman, M., Cirignano, L., Moses, W.W., Derenzo, S.E., Weber, M.J., 2003. $LaCl_3$:Ce scintillator for γ-ray detection. Nucl. Instrum. Methods Phys. Res. Sect. A: Accel. Spectrometers Detect. Assoc. Equip. 505 (1), 76–81. http://dx.doi.org/10.1016/S0168-9002(03)01024-6, Proceedings of the tenth Symposium on Radiation Measurements and Applications.

Sonu, Tyagi, M., Patel, T., Vuong, P.Q., Sarkar, P.S., Kim, H., 2023. Discrimination of fast and thermal neutrons using a novel phoswich detector of $LaCl_3$ and LiI:Eu single crystal scintillators. IEEE Trans. Nucl. Sci. 70 (7), 1325–1330. http://dx.doi.org/10.1109/TNS.2023.3271460.

Vedia, V., Carmona-Gallardo, M., Fraile, L.M., Mach, H., Udías, J.M., 2015a. Performance evaluation of $LaBr_3$(ce) crystal geometries designed for fast timing applications. In: 2015 IEEE Nuclear Science Symposium and Medical Imaging Conference . NSS/MIC, pp. 1–2. http://dx.doi.org/10.1109/NSSMIC.2015.7581832.

Vedia, V., Mach, H., Fraile, L., Udías, J., Lalkovski, S., 2015b. Enhanced time response of 1-in. $LaBr_3$(Ce) crystals by leading edge and constant fraction techniques. Nucl. Instrum. Methods Phys. Res. Sect. A: Accel. Spectrometers Detect. Assoc. Equip. 795, 144–150. http://dx.doi.org/10.1016/j.nima.2015.05.058.

Vuong, P.Q., Kim, H., Luan, N.T., Kim, S., 2021. Neutron spectroscopy using pure $LaCl_3$ crystal and the dependence of pulse shape discrimination on Ce-doped concentrations. Nucl. Eng. Technol. 53 (11), 3784–3789. http://dx.doi.org/10.1016/j.net.2021.05.020.

Vuong, P.Q., Quang, N.D., Kim, H., Lee, J.Y., Kang, S.C., Nam, U.-W., Park, W.-K., Sohn, J., Choi, Y.-J., Youn, S., Ye, S.-J., Kim, S., 2022. Development of novel crystal scintillators for lunar surface science. Radiat. Phys. Chem. 201, 110425. http://dx.doi.org/10.1016/j.radphyschem.2022.110425.